Sains Malaysiana 55(10)(2026): 1626-1638
http://doi.org/10.17576/jsm-2026-5510-03

Synthesis, Characterisation and Density Functional Theory Study of A_4- and A_2B_2-Type Meso-Hexylporphyrin Derivatives and Their Zinc (II) Complexes

(Kajian Teori Fungsian Sintesis, Pencirian dan Ketumpatan bagi Terbitan Meso-Heksilporfirin Jenis A_4- and A_2B_2- serta Kompleks Zink (II)nya)

NABILA SYUHADA ZAILAN[1], YASOTHAA A/P RAMAIYAH[1], NUUR HAZIQAH MOHD RADZUAN[1], MOHD BAKRI BAKAR[2], WAN NURFADHILAH ZAHARIM[1,3] & MUNTAZ ABU BAKAR[1,*]

[1]*Department of Chemical Sciences, Faculty of Science and Technology, Universiti Kebangsaan Malaysia, 43600 UKM Bangi, Selangor, Malaysia*
[2]*Department of Chemical Sciences, Faculty of Science, Universiti Teknologi Malaysia, 81310 UTM Johor Bahru, Johor, Malaysia*
[3]*Nuclear Structure Research Group, RIKEN Nishina Center for Accelerator Based Science, 2-1 Hirosawa, Saitama 351-0198, Wako, Japan*

Received: 21 May 2026/Accepted: 9 September 2026

*Corresponding author; email: muntaz@ukm.edu.my

ABSTRACT

Porphyrin is a macrocylic aromatic compound that has attracted the attention of scientists due to its ability to be tuned for various applications such as photodynamic therapy, catalyst, and DSSC. Understanding the theoretical properties of porphyrin enables electronic tuning for future design, producing efficient functions of porphyrin compounds. An extensive computational study on structural electronic properties of A_4 and A_2B_2 type meso-hexylporphyrin derivatives has yet to be conducted. Therefore, Density Functional Theory method which is a computational study tool was applied in this investigation to study the properties of meso-hexylporphyrin theoretically. In this work, all 4 meso-hexylporphyrin derivatives were synthesised and characterised using Nuclear Magnetic Resonance (NMR) and Ultra Violet-Visible (UV-VIS). Structures were optimized at B3LYP/6-31G(d) and studied based on the structural and electronic properties parameters. From this study, the symmetry and planarity of porphyrin derivatives increase after coordination with the Zn metal complex. Derivatives **1** and **4** were reported to be soft compounds that are more reactive, with a low HOMO-LUMO energy gap, 2.62 eV and 2.74 eV respectively. However, derivatives **3** and **5** are shown as hard compound which are more stable, having a high HOMO-LUMO energy gap, 2.75 eV and 2.91 eV, respectively. This study provides a basis for further exploration of meso-hexylporphyrin as a potential model compound for various applications.

Keywords: DFT study; HOMO-LUMO; macrocyclic aromatic compound; meso-hexylporphyrin

ABSTRAK

Porfirin adalah sebatian aromatik makrosilik yang telah menarik perhatian saintis kerana keupayaannya untuk dioptimumkan kepada pelbagai aplikasi seperti terapi fotodinamik, mangkin dan DSSC. Memahami sifat teori porfirin membolehkan pengubahsuaian elektronik untuk mereka bentuk masa hadapan dan menghasilkan fungsi cekap sebatian porfirin. Kajian pengkomputeran ke atas sifat struktur elektronik mengenai terbitan meso-heksilporfirin jenis A_4 dan A_2B_2 masih belum dijalankan. Oleh itu, kaedah Teori Fungsian Ketumpatan yang merupakan kaedah pengkomputeraan digunakan dalam penyelidikan ini untuk mengkaji sifat terbitan meso-heksilporfirin secara teori. Dalam kajian ini, empat terbitan meso-heksilporfirin telah disintesis dan dicirikan menggunakan analisis Resonans Magnetik Nuklear (RMN) dan Ultra Lembayung Boleh Nampak (ULBN). Struktur telah dioptimumkan pada B3LYP/6-31G(d) dan dikaji berdasarkan parameter sifat struktur dan elektronik. Hasil kajian ini, struktur simetri dan keplanaran terbitan porfirin meningkat selepas pengkoordinatan dengan kompleks logam Zn. Terbitan **1** dan **4** dilaporkan sebagai sebatian lembut yang lebih reaktif tetapi kurang stabil, dengan jurang tenaga HOMO-LUMO yang rendah, masing-masing 2.62 eV dan 2.74 eV. Walau bagaimanapun, terbitan **3** dan **5** ditunjukkan sebagai sebatian keras yang lebih stabil tetapi kurang reaktif, mempunyai jurang tenaga HOMO-LUMO yang tinggi, masing-masing 2.75 eV dan 2.91 eV. Kajian ini menyediakan asas bagi penerokaan lanjut terhadap meso-heksilporfirin sebagai sebatian model yang berpotensi untuk pelbagai aplikasi.

Kata kunci: HOMO-LUMO; kajian DFT; meso-heksilporfirin; sebatian makrosiklik aromatik

INTRODUCTION

Porphura known as porphyrin can be divided into 2 groups; natural and synthetic porphyrin. In nature, porphyrin functions vitally in oxygen transport for heme and light absorption by chlorophyll via the photosynthesis process (Tahoun et al. 2021). Synthetic porphyrin, however, was first introduced by Fischer in 1930 and has been an extensively studied compound by worldwide scientist till this day (Fischer 1930). Interestingly, the structure of porphyrin illustrated in Figure 1, which is a macrocyclic aromatic compound with an extended π conjugated system, allows for modification to be implemented via conjugation with a substitute group or coordination with metal complexes (Lin et al. 2020). The idea was to tune the structure hence their ability to exhibit different structural, electronic and optical properties for various applications such as photodynamic therapy, sensor and DSSC.

The main active site for the modification on the porphyrin is at the meso position, yielding a symmetry or non-symmetry geometry type of porphyrin. The positions for meso are at carbons 5, 10, 15, and 20 at the macrocyclic porphyrin structure shown in Figure 1. Meso active site is more reactive and selective compared to other active sites such as α and β (Vicente & Smith 2014). Modification at this active site had proven to improve the electron density distribution and enhance the photophysical properties of the porphyrin (Bashir, Alotaibi & Clayborne 2024; Nishida et al. 2021). Furthermore, porphyrin is able to conjugate with substituent group such as aromatic groups, a halogen groups or a heterocyclic groups via an electrophilic substitution reaction, halogenation and nitration reactions easily. A_4 and A_2B_2 type of porphyrin is a symmetry porphyrin that has been widely studied among scientists as it provides convenient conjugation reaction.

Substitution with aromatic group such as phenyl was used as a model compound due to its stability and tunability properties (Senge 2011). Meso-tetraphenylporphyrin (TPP) compound has highly stable structure from extended π conjugation allow for modification with other functional groups or metal to enhance the efficiency for the studied application. However, the lack of studies on substitution with an alkyl group provides a gap to establish a fundamental structure-property relationship for future study studies on applications. Studies have shown that an alkyl groups give better solubility and aggregation, especially in applications related to photodynamic therapy, where high solubility improves the efficiency as a photosensitizer compared to phenyl group. Not to mention, a long alkyl chain can also provide steric hindrance to the aromatic structure of porphyrin with its bulky group improving stability and absorbance in the red shift (Higashino et al. 2016). Coordination with metal porphyrin has been reported to improve the structural stability and optical properties of porphyrin for wider application. Zn-porphyrin is more selective than other metal due to its efficiency, stable at high temperature and easily synthesised in organic solvent (Bouicha et al. 2025; Sánchez-Bojorge et al. 2019).

Computational study plays an important role in stabilizing the theoretical and experimental analysis for optimal results (Walker et al. 2013). Density Functional Theory has been widely recognized as a tool for computational study, especially its ability to perform calculations for large compounds and is cost-effective (Baseden & Tye 2014). However, the chosen functional and basis set for calculation will affect the accuracy of the results analysis (Wan Nurfadhilah et al. 2024). Identify the reactivity and behavior of porphyrin compound through the computational studies enables researchers to optimize its properties for specific applications. Modified porphyrin provides different geometrical structure, electronic effect and charge transfer effect. Though numerous studies conducted on meso-aromatic porphyrin recently, fewer study reported

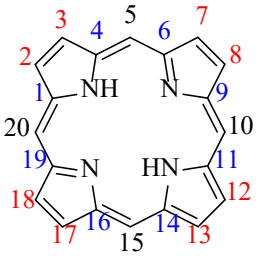


FIGURE 1. Chemical structures and numbering system of the porphyrin compound

on the electronic properties of meso-alkylporphyrin using both experimental and theoretical approaches. Since it is crucial to elucidate the structure and electronic properties of meso-alkylporphyrin, this work will provide a better understanding on how the alkyl group affects the properties of porphyrin.

In this work, four derivatives of meso-hexylporphyrin were synthesised and characterised using Nuclear Magnetic Resonance and Ultraviolet-Visible instrument. The structural and electronic properties, such as HOMO LUMO energy, energy gap, global reactivity and charge distribution were analyzed accordingly from the DFT computational study woth the B3LYP method and 6-31G(d) basis set. The experimental part conducted was used as a model for DFT calculation and to support the validity of the theoretical study. Computational data analysis in this study provides insights into the structure electronic properties and reactivity of the compounds. The finding also helps as theoretical design to support future research on meso-hexylporphyrin as a potential model compound for various applications.

EXPERIMENTAL MATERIALS AND METHODS

MATERIALS

All the materials were analytical grade and purchased from Merck Sdn Bhd and Sigma Aldrich. The chemicals and reagents used for this study were pyrrole 98% (Sigma Aldrich), trifluoroacetic acid 99% (Sigma Aldrich), triethylamine (Merck Sdn Bhd), heptanaldehyde (Sigma Aldrich), paraformaldehyde 95% (Sigma Aldrich), potassium hydroxide 98% (Sigma Aldrich), zinc acetate 99.99% (Sigma Aldrich), 3-dichloro-5,6-dicyano-1,4-benzaquinone 98% (Sigma Aldrich), dichoromethane (Sigma Aldrich), n-hexane 99% (Merck Sdn Bhd) and methanol (Merck Sdn Bhd).

INSTRUMENTATION

Thin-layer chromatography (TLC) was run on a 0.2 mm silica gel GF254 (Merck Sdn Bhd) on an aluminium plate and spots were detected using UV light. Nuclear Magnetic Resonance ^{1}H and ^{13}C analysis were performed on a Bruker FT-NMR 400 MHz and 100 MHz instrument (Bruker BioSpin GmbH, Rheinstetten, Germany) for ^{1}H NMR and ^{13}C NMR, respectively. Samples were dissolved in deuterated chloroform solvent ($CdCl_3$-D1) before analysis. The resulting chemical shifts were measured in unit ppm with reference to trimethylsilane (TMS) at a chemical shift of 0.00 ppm.

Absorption spectra were obtained using Shimadzu Spectrophotometer (UV-1650, Shimadzu Corporation, Kyoto, Japan) instrument. All samples were dissolved in 2×10^{-6} M dichloromethane (DCM) solvent. Compounds were measured between 350 and 700 nm wavelength range.

PREPARATION OF COMPOUNDS

Synthesis of 5,10,15,20-tetrahexylporphyrin **(1)** were according to Nuur Haziqah et al. (2021). 5 mL pyrrole and 7.60 mL heptanaldehyde were added to a clean round bottom flask equipped with a stir bar under reflux conditions. A small amount of 0.1 mL acid catalyst, trifluoroacetic acid were added into the flask. Reactions were left at room temperature for 18 h. Then, 3-dichloro-5,6-dicyano-1,4-benzaquinone (DDQ) (2 g, 8.80 mmol) was added to allow for the oxidation reaction to take place for another 1 h before the reaction were quenched with 5 mL triethylamine. The mixture was separated using Liquid Vacuum Chromatography through silica gel and dichloromethane as eluent. The combined organic layers were evaporated using a rotary evaporator and recrystallized from dichloromethane/methanol. Solid crystal was washed with methanol yielding purple color crystal. The crystals were isolated and stored for characterisation. Color: Purple (450 mg, 3%), ^{1}H NMR ($CdCl_3$-D1, 100 MHz): δ ppm -2.62 (s, 2H), 1.03 (t, 12H, J_{HH} = 1.8 Hz), 1.51 (m, 8H), 1.61 (m, 8H), 1.85 (m, 8H), 2.56 (m, 8H), 4.93 (t, 8H, J_{HH} = 2.0 Hz), 9.47 (s, 8H); ^{13}C NMR ($CdCl_3$-D1, 400 MHz): δ ppm 14.22, 22.83, 30.34, 31.33, 35.56, 38.72, 118.39; UV-VIS (CH_2Cl_2): λ_{max} (nm) 418, 520, 555, 659.

Synthesis of Dipyrromethane **(2)** were prepared according to Nuur Haziqah et al. (2026). To a clean three-neck round bottom flask equipped with a magnetic stirrer in a reflux condition, paraformaldehyde (5 g, 166.52 mmol) and 200 mL were added. After the temperature reached 60 ºC, 0.80 mL of trifluoroacetic acid was added quickly. Dark colour with a sudden 10 to 15 ºC temperature increase was observed. Mixture was maintained under 90 ºC. After 30 min, potassium hydroxide (0.80 g in 30 mL distilled water) was added and left to stir for 18 h at room temperature. Mixture was separated through silica gel and dichloromethane as eluent using Liquid Vacuum Chromatography. Next, samples were evaporated with a rotary evaporator and purified using Kugelrohr (5 ºC temperature increment until maximum temperature 180 ºC, 20 rpm). Color: Light yellow (6 g, 38%), ^{1}H NMR ($CdCl_3$-D1, 100 MHz): δ ppm 3.98 (s, 2H), 6.07 (dd, 2H), 6.17 (s, 2H), 6.66 (s, 2H), 7.80 (s, 2H). The NMR data are consistent with previously reported in the literature (Nuur Haziqah et al. 2021).

Synthesis of 5,15-dihexylporphyrin **(3)** were prepared according to Nuur Haziqah et al. (2021). Prior to synthesis of derivative **3**, dichloromethane was added with phosphorus pentoxide and undergo distillation reaction to prepare a dry dichloromethane (Williams & Lawton 2010). A three-neck round bottom flask covered with aluminium foil with a stir bar was flushed with nitrogen gas to create an inert condition. Compound **2** (1 g, 6.84 mmol) and 0.80 mL heptanaldehyde were added to the flask filled with 700 mL dry dichloromethane in a reflux conditions. Then, 0.10 mL trifluoroacetic acid were added into the flask before left to stir for 18 h at

room temperature. After 18 h, 3-dichloro-5,6-dicyano-1,4-benzaquinone (DDQ) (2.50 g, 11.01 mmol) was added to allow for the oxidation reaction to take place for another 1 h before the reaction was quenched with 5 mL triethylamine (Nuur Haziqah et al. 2021). The mixture was separated, evaporated and recrystallized following the same procedure used for compound **1**. Color: Purple (360 mg, 23%), ^{1}H NMR ($CdCl_3$-D1, 100 MHz): δ ppm -2.92 (d, 2H), 0.97 (t, 6H, J_{HH} = 1.9 Hz), 1.43 (m, 4H), 1.56 (m, 4H), 1.85 (m, 4H), 2.57 (m, 4H), 5.01 (t, 4H, J_{HH} = 2.0 Hz), 9.41 (d, 4H, $^{3}J_{HH}$ = 1.1 Hz), 9.57 (d, 4H, $^{3}J_{HH}$ = 1.2 Hz), 10.16 (s, 2H); UV-VIS (CH_2Cl_2): λ_{max} (nm) 404, 501, 534, 577, 629. The NMR data are consistent with previously reported in the literature (Nuur Haziqah et al. 2021).

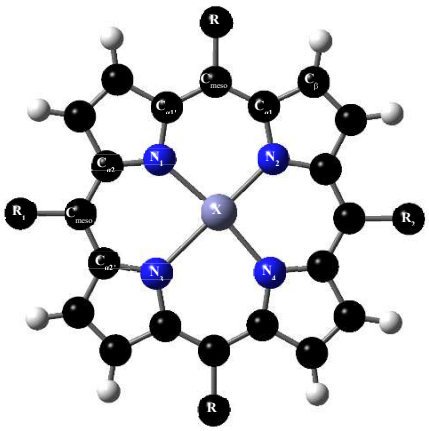
General procedure for the synthesis of meso-Zn-porphyrin were according to Nuur Haziqah et al. (2021). 0.10 mmol porphyrin compound and 0.27 mmol zinc acetate, $Zn(OAc)_2$ were added into a round bottom flask partially immersed in silicon oil filled with 10 mL chloroform. The reaction was stirred and heated at 60 ºC and the progress of the reaction was monitored by TLC using dichloromethane/hexane (1:1) as eluent. After 15 min, the mixture was evaporated and separated using flash column chromatography through silica gel and dichloromethane/ n-hexane as eluent. Samples were evaporated using a rotary evaporator and recrystallized from dichloromethane/methanol (Nuur Haziqah et al. 2021).

Zn[5,10,15,20-tetrahexylporphyrin] **(4)** were synthesised from reaction between compound **1** (50 mg, 0.10 mmol) and $Zn(OAc)_2$ (50 mg, 0.27 mmol). Color: reddish purple (60 mg 68%). ^{1}H NMR ($CdCl_3$-D1, 100 MHz): δ ppm 0.94 (m, 4H, J_{HH} = 1.8 Hz), 1.36 (m, 8H), 1.45 (m, 8H), 1.59 (m, 8H), 2.27 (m, 8H), 4.49 (t, 8H, J_{HH} = 2.0 Hz), 9.26 (s, 8H); ^{13}C NMR ($CdCl_3$-D1, 400 MHz): δ ppm 13.08, 21.63, 29.00, 30.75, 32.91, 36.16, 115.80, 128.63, 140.09; UV-VIS (CH_2Cl_2): λ_{max} (nm) 420, 558, 618.

Zn[5,15-dihexylporphyrin] **(5)** were synthesised from reaction between compound **3** (50 mg, 0.10 mmol) and $Zn(OAc)_2$ (50 mg, 0.27 mmol). Color: reddish purple (50 mg, 63%). ^{1}H NMR ($CdCl_3$-D1, 100 MHz): δ ppm 0.94 (t, 6H), 1.40 (m, 4H), 1.49 (m, 4H), 1.68 (m, 4H), 2.39 (m, 4H), 4.69 (t, 4H, J_{HH} = 2.0 Hz), 9.18 (d, 4H, $^{3}J_{HH}$ = 1.2 Hz), 9.45 (d, 4H, $^{3}J_{HH}$ = 1.2 Hz), 9.72 (s, 2H); UV-VIS (CH_2Cl_2): λ_{max} (nm) 406, 536. The NMR data are consistent with previously reported in the literature (Nuur Haziqah et al. 2021).

COMPUTATIONAL TECHNIQUE

A computational study was performed using Gaussian16 computational software, with B3LYP/6-31G(d) functional and basis set. B3LYP is a hybrid functional of Becke's three-parameter exchange functional with Lee-Yang-Parr correlation functional, which has been commonly used for the study of organic structure (Becke 1993; Lee, Yang & Parr 1988). 6-31G(d) is a double-zeta basis set with polarization functions (for C, H, N, Zn). Previous studies had proven to produce results closer to experimental data and had shown acceptable accuracy for structural electronic properties analysis for both free base and metal Zn porphyrin for this specific basis set (Kuan et al. 2025). Hence, 6-31G(d) were used in the study for the same structural electronic properties study using DFT and is sufficient enough. Chosen functional and basis set shown no symmetry constrain. As illustrated in Figure 2, the meso-hexylporphyrin derivatives were investigated by different types of porphyrin (A_4 and A_2B_2) with metal Zn. Hexyl group attaches to all meso positions 5, 10, 15, and 20 producing an A_4 type meso-porphyrin; meanwhile hexyl group attach to the meso position 5 and 15 producing an A_2B_2 type porphyrin. Structure for all the compound is illustrated in the list of meso-hexylporphyrin derivatives in the Supporting Information (data not provided).



X = H, Zn
R = C_6H_{13}
R_1 = C_6H_{13}, H
R_2 = C_6H_{13}, H

FIGURE 2. Labelling diagram for porphyrin structure with hexyl group substituent and metal zinc (Zn)

All structures were optimized at the lowest energy before analyzing the structural properties to identify the stability of the structure. Bond length and bond angle were the parameters for the structural analysis. Electronic analysis was calculated at Single Point Energy in the gaseous state using the same functional and basis set. Parameters for electronic study include HOMO and LUMO energy, energy gap, global reactivity and charge distribution. Formula for the global reactivity includes calculation on chemical potential (μ), global hardness (η), global softness (σ), electrophilicity index (ω) and electronegativity (χ) according to Equations (2) – (6), respectively. Energy gap calculation obtained from Equation (1). GaussView 6.0 software was used to visualized and generated the molecular orbital.

$$\Delta E_g = E_{LUMO} - E_{HOMO} \quad (1)$$

$$\mu = \frac{(E_{HOMO} + E_{LUMO})}{2} \quad (2)$$

$$\eta = \frac{(E_{LUMO} - E_{HOMO})}{2} \quad (3)$$

$$\sigma = \frac{1}{\eta} \quad (4)$$

$$\omega = \frac{\mu^2}{2\eta} \quad (5)$$

$$\chi = - \frac{(E_{HOMO} + E_{LUMO})}{2} \quad (6)$$

$$E_g = \frac{hc}{\lambda_{cutoff}} \quad (7)$$

RESULTS AND DISCUSSION

SYNTHESIS

Synthesis of A_4 and A_2B_2 meso-hexylporphyrin were performed according to Lindsey method (Lindsey 2010; Lindsey et al. 1987). A_4 type porphyrin was synthesised via one-pot synthesis; condensation and oxidation reaction. A condensation reaction between pyrrole and heptanaldehyde was conducted for 18 h at room temperature in the presence of an acid catalyst. Further, oxidation reaction takes place with the oxidizing agent and triethylamine to stop the reaction yielded derivative **1**. To synthesise derivative **3** which is an A_2B_2 type porphyrin, intermediate **2** was first synthesised from the reaction between pyrrole and paraformaldehyde with trifluoroacetic acid catalyst. Then, a similar procedure for derivative **1** was conducted by changing pyrrole to intermediate **2** yielded derivative **3**. Derivatives **1** and **3** undergo coordination with metal Zn at the center of the porphyrin aromatic ring. Reactions were conducted with the addition of excess zinc acetate to porphyrin sample dissolved in chloroform solvent to yield derivatives **4** and **5,** respectively. The identities of all the compounds were confirmed by ^{1}H NMR and ^{13}C NMR spectroscopy. However, few compounds shown relatively low yield that may happen due to product loss during purification process and the sensitivity of the compound towards light. The compounds were also characterised with UV-Visible spectroscopy, which explains the Soret Band and Q band absorption. Reaction schemes are illustrated in the Supporting Information (data not provided).

NUCLEAR MAGNETIC RESONANCE SPECTROSCOPY

All desired peak signals for the compounds are shown in the Supporting Information (data not provided). Macrocyclic aromatic porphyrin structures exhibit magnetic anisotropy effects due to their extended π-conjugation. In proton NMR spectrum, intermediate **2** produces three signals δ 6.661, 6.174 and 6.074 ppm, which are attributed to protons in the pyrrole ring while the signal at δ 3.984 ppm is upfield are referring to protons in the methylene (CH_2) group. The signal for the CH_2 group is more upfield due to the proton position in the shielding of the induced magnetic field. At the most deshielded region, a broad signal of δ 7.796 ppm is for the protons bonded to the nitrogen atom in the pyrrole ring.

Derivatives **1**, **3**, **4**, and **5** demonstrated nearly identical NMR spectra due to the structure and the position of the substituent. A singlet peak signal at around δ -2 to -3 ppm shows the proton bonded to the nitrogen in the aromatic porphyrin structure. This is only observed for free base meso-porphyrin which are derivatives **1** and **3**. The disappearance of the peak at this signal in derivatives **4** and **5** explains the formation of bonds between metal Zn with the N atom at the porphyrin core from the coordination reaction. The signals at around δ 0.9 to 5 ppm indicate the protons at the substituted hexyl group labeled as H21, H22, H23, H24, H25, and H26. Signal for H21 is slightly shifted downfield due to the methyl (CH_3) group being positioned far from the aromatic porphyrin ring and experiencing a weaker magnetic field. The signals observed at the deshielded region around 9 to 10 ppm is the proton at the β position which is located at the pyrrole group. For highly symmetrical A_4 type porphyrin derivatives **1** and **4**, the peak appears as a singlet at δ 9.465 and 9.260 ppm, respectively, while A_2B_2 type porphyrin is detected as two doublets peak. Signals at δ 9.574 and 9.407 ppm for derivative **3** with δ 9.453 and 9.183 ppm for derivative **5**. An enhancement in the number of signals for proton at the β position is observed due to the chemical environment (substituent) at the meso position. An additional singlet signal was observed at the most deshielded region δ 10.160 and 9.718 ppm for the proton bonded at meso position in derivatives **3** and **5**.

The ^{13}C NMR was performed on derivatives **1** and **4** to further verify the proposed structure. Carbon at position α, β, meso and hexyl group were identified as a singlet peak. Signal at between δ 13.01 and 38.72 ppm are relatively explain the presence of carbon in the hexyl group at the meso position. The signals correspond to the carbon at α, β, meso are detected at higher ppm in the deshielded region. However, no signal for carbon at position α and β for derivative **1** observed due to a weak signal.

UV-VISIBLE ABSORPTION SPECTRA

The electronic absorption spectra of compound **1**, **3**, **4**, and **5** were characterised in dichloromethane at room temperature. Two major band observed for porphyrin which are Soret Band and Q Band allows to explain the electronic properties of porphyrin (Aderne et al. 2022). Soret Band is measured at low wavelength value with high intensity between 300-450 nm while Q band is measured at high wavelength value with low intensity between 500-750 nm for the energy transition from π⟶ π* according to Goutterman four orbital model (Giovannetti 2012). From the data analysis, the energy gap for the derivatives can be calculated following Equation (7) derived and the graphical determination of λ_{cutoff} value is presented in the Supporting Information (data not provided).

Figure 3 shows a UV-Visible spectra for all derivatives. Free base meso-porphyrin exhibit 4 distinct Q-bands measured at high wavelength value due to its lower symmetry (D_2h symmetry). Coordination with metal Zn improves the symmetry (D_4h symmetry) causing the splitting peaks to be reduce to 2 distinct Q-bands. Based on data analysis in Figure 3, Soret Band can be observed at around 404 to 420 nm with strong intensity peak for all derivatives. Higher peak value (batochromic shift) can be observed for derivatives **1** and **4** due to electron inductive effect from the hexyl group bonded to all meso position which improve the density towards the macrocycle structure. Only three distinct Q-bands were observed for derivative **1** while the fourth Q-band transition may remain unresolved due to its weak intensity under the stated measurement conditions. However, coordination with metal Zn at the core porphyrin improve the geometrical structure for both A_4 and A_2B_2 meso-porphyrin compound, showing higher absorption value compared to free base meso-porphyrin. Reduce number of splitting peak at the high region confirmed that the coordination with metal Zn occur in derivatives **4** and **5**. Calculated energy gap is presented in Table 1. Steric effect and stability of compound from the symmetrical geometry influence the electronic properties of the derivatives. Comparing between A_4 type and A_2B_2 type meso-hexylporphyrin, derivatives **1** and **4** showing lower energy gap, 1.85 eV and 1.93 eV, respectively, compared to derivatives **3** and **5**.

STRUCTURAL ANALYSIS

All optimized structures shown in Figure 4, which were conducted at the lowest energy. Based on the structure shown, the planarity of the porphyrin does not change after coordination with metal Zn. However, the conjugation with the hexyl group causes steric deviations to occur from the aromatic macrocyclic porphyrin plane. This is a normal response for a bulky group, such as hexyl group. It reduces the steric constraints between the hydrogen at C21 and the hydrogen at $C_β$.

Calculated bond length and bond angle of meso-hexylporphyrin are listed in Tables 2 and 3, respectively. The N-N bond length is 4.08-4.09 Å, and after coordination with Zn, the Zn-N bond length is between 2.04-2.05 Å. The decreasing trend in bond length after

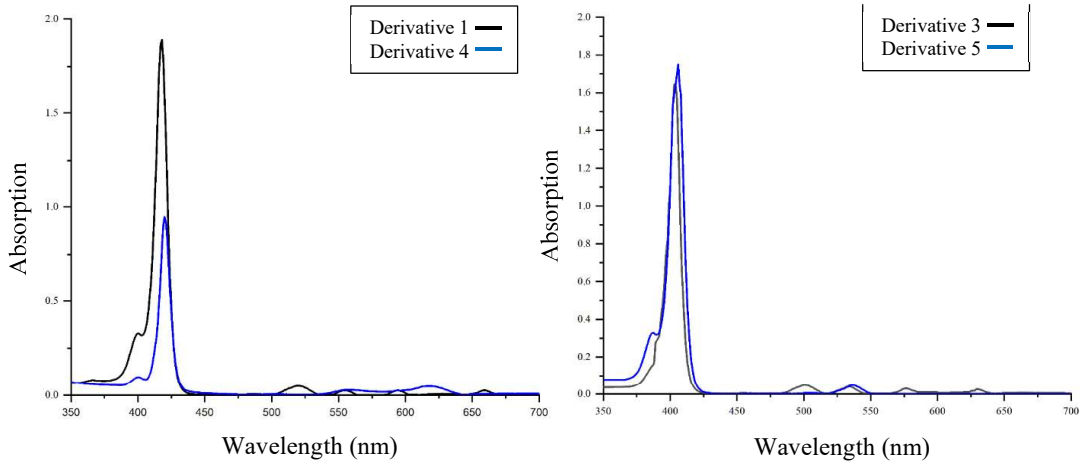


FIGURE 3. UV-Visible absorption spectra of derivatives A_4 type meso-porphyrin (derivatives **1** and **4**) and A_2B_2 type meso-porphyrin (derivatives **3** and **5**)

TABLE 1. Absorption spectrum and energy gap value for meso-hexylporphyrin derivatives

Derivative	λ_{max} (nm) Soret Band	λ_{max} (nm) Q band	λ_{cutoff} (nm)	E_{gap} (eV)
1	418	520, 555, 659	672	1.85
4	420	558, 618	643	1.93
3	404	501, 534, 577, 629	638	1.94
5	406	536	551	2.25

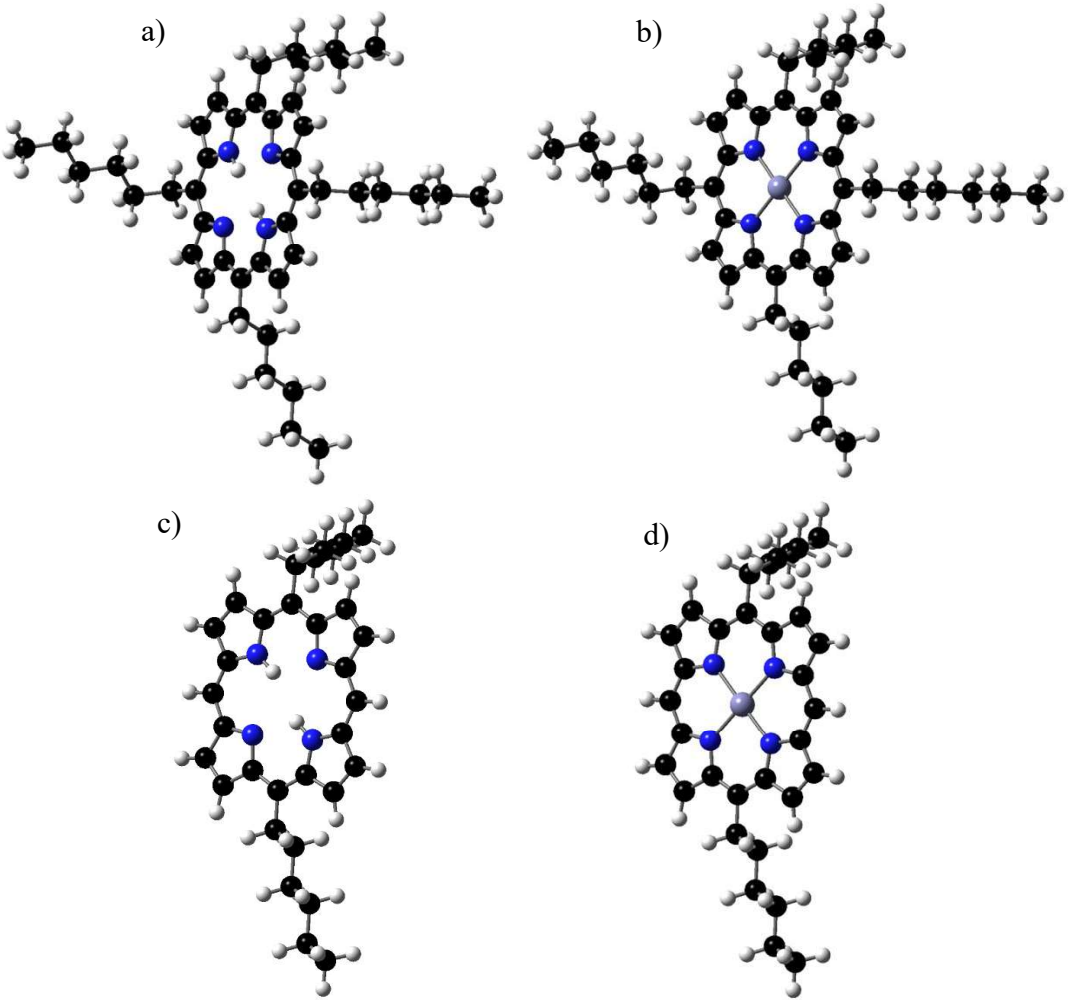


FIGURE 4. Optimized structure of meso-hexylporphyrin derivatives calculated at B3LYP/6-31G(d). (a) Derivative **1** (b) Derivative **4** (c) Derivative **3** and (d) Derivative **5**

TABLE 2. Bond length (Å) for meso-hexylporphyrin derivatives calculated at B3LYP/6-31G(d)

Derivative	N-N	N-H	N-C_α	C_α-C_β	C_α-C_{meso}	C_{meso}-C_{21}	C_β-C_β	Zn-N
1	4.08	1.02	1.37	1.46	1.41	1.52	1.35	-
4	4.09	-	1.39	1.45	1.41	1.52	1.37	2.04
3	4.09	1.02	1.37	1.46	1.41	1.52	1.36	-
5	4.08	-	1.38	1.45	1.41	1.52	1.36	2.05

TABLE 3. Bond angle (A) and dihedral angle (D) for meso-hexylporphyrin derivatives calculated at B3LYP/6-31G(d)

Derivative	**1**	**4**	**3**	**5**
D($C_{\alpha,}$ Cmeso, C_{21}, C_{22})	88.04°	88.98°	87.41°	89.05°
A(Cmeso, $C_{\alpha,}$, N_{α})	126.82°	126.57°	124.95°	126.01°
A($C_{\alpha1,}$ Cmeso, $C_{\alpha1'}$)	124.70°	124.23°	122.77°	123.55°
A($C_{\alpha2,}$ Cmeso, $C_{\alpha2'}$)	124.71°	124.23°	129.69°	127.21°
A($C_{\alpha,}$ N, C_{α})	105.90°	106.96°	105.85°	106.74°

coordination with metal Zn is due to the increasing symmetry geometry of Zn-porphyrin. The highly symmetrical geometry can be confirmed by increasing the bond angle between $C_{\alpha,}$ N, C_{α} for metal porphyrin, which are 106.96° and 106.74° for ZnTHP and ZnDHP in comparison to 105.90° and 105.85° for THP and DHP. Bond length surrounding the macrocyclic plane showing similarity for all compound especially at N-C_{α}, C_{α}-C_{β}, C_{meso}-C_{21} and C_{β}-C_{β}. The hexyl group rotates out of plane at meso position 88.04° and 87.41° for free base porphyrin, also 88.98° and 89.05° for metal porphyrin. The rotating of hexyl group is to relieve steric strain and prevent steric deviations from occurring. According to Zhang et al. (2025), the increasing symmetry geometry after coordination with zinc metal causing meso-arylporphyrin structure to be out of plane. Function of substituent can be identified from the dihedral angle between Cmeso, C_{α}, N_{α}, whereby electron withdrawing tends to decrease the Cmeso, C_{α}, N_{α} but increases the angle $C_{\alpha1}$-Cmeso-$C_{\alpha1'}$ and $C_{\alpha2}$-Cmeso-$C_{\alpha2'}$ (Barbee & Kuznetsov 2012). Electron acceptor reacts otherwise. Based on Table 2, it is shown that the hexyl group can act as an electron acceptor due to a higher dihedral angle between Cmeso, C_{α}, N_{α} and lower bond angle between $C_{\alpha1}$-Cmeso-$C_{\alpha1'}$ and $C_{\alpha2}$-Cmeso-$C_{\alpha2'}$.

ELECTRONIC ANALYSIS

HOMO and LUMO Plot

HOMO and LUMO explain on which electron acts as the electron donor and electron acceptor. Highest Occupied Molecular Orbital or HOMO acts as an electron donor while the Lowest Occupied Molecular Orbital or LUMO acts as an electron acceptor (Dhifaoui et al. 2021). Figures 5 and 6 show the HOMO and LUMO plots obtained from GaussView software. The red and green color shown on the structure signifies the positive and negative iso-surfaces, respectively. Based on Figures 5 and 6, the orbital density for HOMO mostly localizes at the center of the porphyrin aromatic macrocyclic structure, while LUMO shows orbital localization at hexyl group. This explains that electron transfer occurs from the porphyrin system towards the constituent hexyl group. Metal Zn has a closed-shell nature with a d^{10} configuration, which affects the localization of electrons at the Zn center of the porphyrin structure. A very small amount and insignificant electron density were observed at the Zn metal center due to the configuration of the metal Zn.

HOMO LUMO Energy and Energy gap

Figure 7 shows the HOMO and LUMO energy and HOMO-LUMO energy gap for all derivatives. The difference between HOMO and LUMO will create an energy gap, enabling the identification of the reactivity of a compound. Energy gap can be calculated from Equation (1). For all derivatives, HOMO energy was calculated between -4.75 eV and -5.00 eV and LUMO energy was calculated between -2.09 eV and -2.18 eV. Both derivatives **1** and **4** structure have four hexyl group bonded at the meso position which is a type A_4. However, for derivatives **3** and **5**, both have two hexyl group bonded at the meso position in trans conformation which is a type A_2B_2.

The HOMO-LUMO energies for free base meso-hexylporphyrin which are derivatives **1** and **3** were calculated at -2.13 eV and -2.18 eV for HOMO also -4.75 eV and -4.93 eV for LUMO, respectively. Derivative **1** showing higher HOMO value indicating that the compound acts as better electron donating towards the porphyrin system. This also influence from the number of substituents attached at the meso position causing steric effect and bulkiness at the substituent. The results also correlate with Zn meso-hexylporphyrin whereby derivative **4** showing higher HOMO value and acts as electron donating group better than derivative **5**.

Based on data in Figure 7, comparing between free base meso-hexylporphyrin derivatives **1** and **3**, derivative **1** exhibit higher HOMO value and smaller LUMO value creating a small energy gap calculated at 2.62 eV. From the experimental UV-VIS data, energy gap for derivatives **1** and **3** were calculated at 1.85 eV and 1.94 eV at the Q band region. The experimental and theoretical data aligns as it shows that derivative **1** showing lower energy gap compared to derivative **3**. The lower HOMO-LUMO energy gap, the higher reactivity of the compound with less stability. This explains that

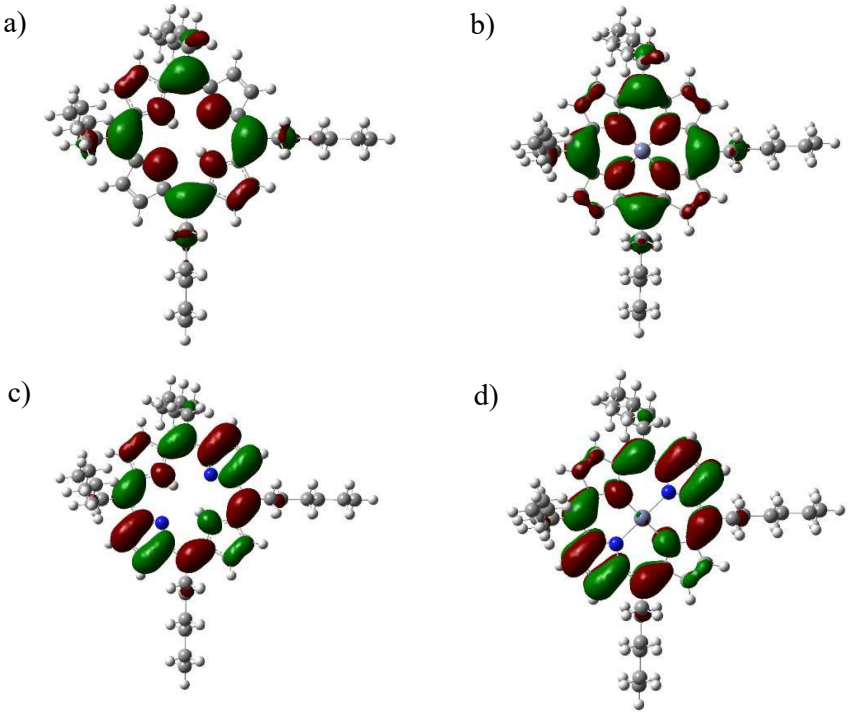


FIGURE 5. HOMO plot for derivative a) **1** and b) **4** with LUMO plot for derivative c) **1** and d) **4**

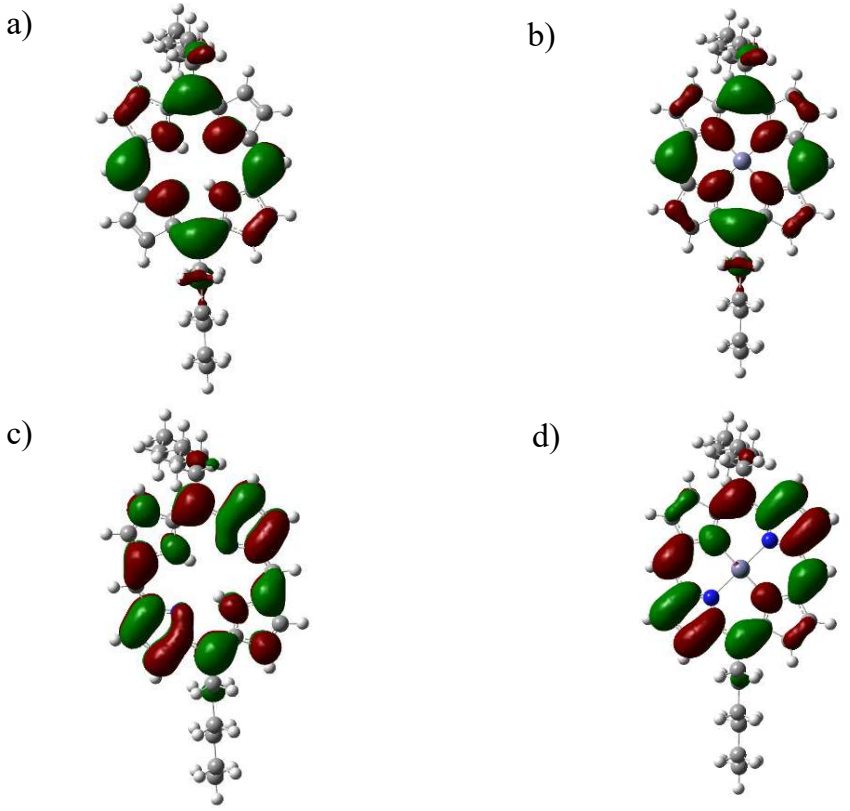


FIGURE 6. HOMO plot for derivative a) **3** and b) **5** with LUMO plot for derivative c) **3** and d) **5**

derivative **1** is more reactive than derivative **3** due to a higher number of conjugations with hexyl group which create a steric effect on the porphyrin structure and improving the reactivity of the compound. The same observation found in metal Zn meso-hexylporphyrin derivatives **4** and **5** where derivative **4** is more reactive than derivative **5** with lower energy gap calculated at 2.74 eV theoretically and 1.93 eV experimentally. Qu et al. (2024) found that addition of electron withdrawing groups attached to the meso position will reduce the energy gap and increasing the reactivity of the compound. This also explains that though derivatives **1** and **4** is more reactive, derivatives **3** and **5** are more stable compound.

The HOMO-LUMO gap calculated in the gas phase is consistently larger than the experimental optical gap obtained from the Q-band absorption in dichloromethane, with differences of 0.77, 0.81, 0.81, and 0.66 eV for derivatives **1**, **3**, **4**, and **5**, respectively. This discrepancy is attributed to the absence of solvent stabilisation in the gas-phase single-point calculation. Dichloromethane, being a moderately polar and polarizable solvent (relative permittivity ~ 8.9), preferentially stabilises the more diffuse and polar LUMO relative to the HOMO through solute-solvent electrostatic interactions, which narrows the experimentally observed gap relative to the vacuum value. As gas-phase calculations neglect this solvation stabilisation, the calculated gap is systematically overestimated relative to solution-phase measurements, consistent with the trend observed across all derivatives in Table 1. Notably, the magnitude of this offset is comparable across the four derivatives, indicating that it arises predominantly from the solvent environment rather than from differences in molecular structure. This supports the validity of the relative reactivity trends (derivatives **1** vs **3**, and **4** vs **5**) discussed in this work, despite the absolute gap values being shifted by the gas-phase approximation. Explicit treatment of the dichloromethane environment, for example through an implicit polarizable continuum model (PCM/CPCM) applied as a single-point correction to the optimized gas-phase geometries, would be expected to narrow this offset further and is recommended as a refinement in future studies of this derivative series.

Global Reactivity Index

Multiple parameters for global reactivity were calculated such as chemical potential (μ), global hardness (η), global softness (σ), electrophilicity index (ω) and electronegativity (χ) to support the HOMO LUMO energy data analysis mentioned earlier. The following calculated values are tabulated in Table 4.

Global softness (σ) and global hardness (η) explains the reactivity of a compound (Parr & Pearson 1983). Free base meso-porphyrin shows that derivatives **1** and **4** have higher σ value than η value. This shows that both compounds exhibit as soft compound, which are more reactive but less stable. This data aligns with the energy gap value whereby derivatives **1** and **4** produce a smaller energy gap which explains the high reactivity comparing to derivatives **3** and **5**. Derivatives **3** and **5** on the other hand, exhibit as a hard compound which is less reactive but more stable. This also correlates with the previous HOMO-LUMO energy gap data, which shows that both compounds produce a higher energy gap.

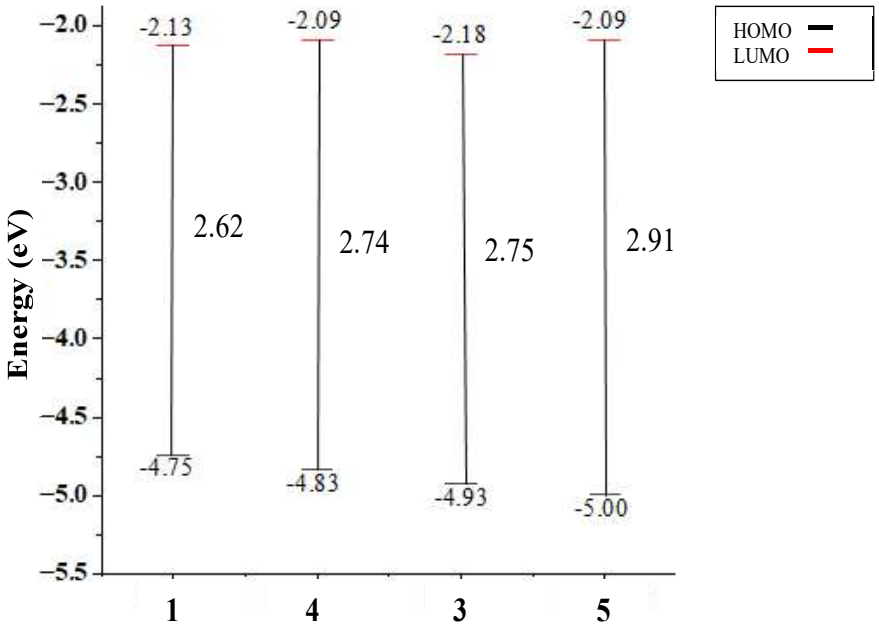


FIGURE 7. HOMO-LUMO energy and energy gap for meso-hexylporphyrin derivatives calculated at B3LYP/6-31G(d)

Chemical potential (μ), electrophilicity index (ω) and electronegativity (χ) explains the ability for the compound to donate or accept electron (Bashir, Alotaibi & Clayborne 2024). Derivatives **1** and **4** also show a higher μ value which are -3.44 eV and -3.46 eV. Lower value χ for derivatives **1** and **4** derivatives defines that the ability for this compound to donate electron, meanwhile, higher value of ω for derivatives **3** and **5** indicates the ability for both compounds to accept electron.

Charge distribution

Table 5 shows the charge distribution for all derivatives. The figure for atomic charge distribution can be obtained in the Supporting Information (data not provided). Based on Table 5, the charge distribution of the N atom shows a more negative value. The N2 and N4 which is an atom bonded directly to H atom in the porphyrin core showing more negative value compared to N1 and N3 atom. It is also confirmed that the increasing trend in N atom from -0.5218 in derivative **1** to -0.5253 in derivative **3** showing the ability for derivative **1** to act as electron donating group better than derivative **3**. The decreasing trend of atomic charge can be observed at C_α and C13 supports the above statement. C_α which is directly bonded to the N atom, gives a more positive value because it is involved in electron delocalization in the macrocyclic ring of the porphyrin. -0.2617, -0.2656, -0.2624, and -0.2581 are atomic charge for C_β on the pyrrole ring for derivatives **1**, **4**, **3**, and **5**, respectively. Results show a more negative charge distribution value because it is not directly involved in electron delocalization. The hexyl group gives a more negative charge distribution value compared to the meso carbons (C13, C18, C23, and C24). This explains that the hexyl group does not involve in delocalized electrons with the parent porphyrin compound and only involves localized delocalization. Therefore, because of this, the macrocyclic structure of the porphyrin gives a more positive value compared to the hexyl group and increases its group density only. The data correlates with the NMR analysis whereby, the hexyl group is situated at more upfield

TABLE 4. Global reactivity value from formula (1)-(5) for meso hexyl derivatives calculated at B3LYP/6-31G(d)

Derivative	μ (eV)	η (eV)	σ (eV)	ω (eV)	χ (eV)
1	-3.444	1.306	0.766	4.541	3.444
4	-3.457	1.372	0.729	4.357	3.457
3	-3.555	1.378	0.726	4.586	3.555
5	-3.546	1.459	0.686	4.310	3.546

TABLE 5. Charge distribution for meso-hexylporphyrin derivatives calculated at B3LYP/6-31G(d)

Atom	1	3	Atom	4	5
N1	-0.5218	-0.5253	N1	-0.6424	-0.6508
N2	-0.5643	-0.5706	N2	-0.6410	-0.6496
N3	-0.5178	-0.5234	N3	0.6383	-0.6488
N4	-0.5643	-0.5707	N4	-0.6409	-0.6504
C_α(C11)	0.1637	0.1643	C_α(C11)	0.1620	0.1745
C_β(C10)	-0.2617	-0.2656	C_β(C10)	-0.2624	-0.2581
C_{meso}(C13)	-0.0364	-0.0359	C_{meso}(C13)	-0.0193	-0.0359
C_{meso}(C18)	-0.0261	-0.2349	C_{meso}(C18)	-0.0106	-0.2284
C_{meso}(C23)	-0.0363	-0.2381	C_{meso}(C23)	-0.0192	-0.2322
C_{meso}(C24)	-0.0261	-0.0292	C_{meso}(C24)	-0.0106	-0.0292
C27	-0.4630	-0.4631	C25	-0.4789	-0.4633
C46	-0.4632	-0.4641	C44	-0.4793	-0.4640
C65	-0.4627	-	C63	-0.4788	-
C83	-0.4629	-	C81	-0.4789	-
			Zn	1.2906	1.2819

region in comparison to the porphyrin system which is more shielded. Coordination with Zn metal at the center of the porphyrin compound gives positive charge distribution values of 1.2906 and 1.2819, which serve as sites for electron transfer to occur. Zn metal having a lone pair allows for sharing of electrons with the N atom from the pyrrole group to form metal porphyrin. N atom gives a negative charge showing that sharing electron and electron distribution occur with the Zn metal.

CONCLUSIONS

The modification on free base A_4 and A_2B_2 type meso-porphyrin with hexyl group were synthesised following Lindsey and MacDonald Condensation [2+2] method yielding derivative **1** and **3**. Upon treatment on derivatives **1** and **3** with excess $Zn(OAc)_2$ in chloroform yielded derivatives **4** and **5**. All derivatives were characterised by NMR Spectroscopy and UV-VIS Absorption Spectroscopy. In conjunction to that, the structural electronic properties of A_4 and A_2B_2 type meso-hexylporphyrin derivatives had been studied via DFT method at B3LYP/6-31G(d) level. Modification with hexyl group and coordination with a metal complex provides different structural and electronic properties. Decreasing trend in bond length calculated for free base meso-porphyrin (4.08 – 4.09 Å) to metalloporphyrin (2.04 – 2.05 Å) showing increasing planarity of the compound. The planarity and symmetry geometry improvement after coordination with metal Zn is important for application in Photodynamic Therapy (PDT), catalyst or sensor. In electronic perspective, the energy gap shows that derivatives **1** and **4** to be more reactive and less stable compound, which are 2.62 eV and 2.74 eV, respectively, due to higher number of conjugations of hexyl group. The observation also aligns for metalloporphyrin derivatives. Derivatives **1** and **4** also shown to be a soft compound consistent with the smaller energy gap. Modification with hexyl group however does not improve the electron density of the porphyrin system as it shows the atomic charge to be more negative than the aromatic macrocyclic parent porphyrin system. It confirms its ability to act as electron withdrawing group as the transfer of electron from the positive to negative. Finding from Qu et al. (2024) stated that the electron withdrawing group pull the electron density towards itself which also shown in the decreasing energy gap. However, with modification, with hexyl group at four meso position in derivatives **1** and **4**, it improves the electron density for the system better than derivatives **3** and **5**. These findings provide insights into the structural electronic study of a long chain meso-porphyrin for future research and improvement.

ACKNOWLEDGEMENTS

We gratefully acknowledge Universiti Kebangsaan Malaysia and RIKEN Nishina Center for Accelerator Based Science for providing the research facilities. This work has been carried out with the support of Malaysian Government through Ministry of Science and Technology Innovation grant FRGS/1/2019/STG01/UKM/02/18. We would also like to thanked CRIM for the NMR Analysis data acquisition. All supplementary data is available upon requests from the corresponding author.

REFERENCES

Aderne, R.E., Borges, B.G.A.L., Ávila, H.C., Von Kieseritzky, F., Hellberg, J., Koehler, M., Cremona, M., Roman, L.S., Araujo, C.M., Rocco, M.L.M. & Marchiori, C.F.N. 2022. On the energy gap determination of organic optoelectronic materials: The case of porphyrin derivatives. *Materials Advances* 3(3): 1791-1803.

Barbee, J. & Kuznetsov, A.E. 2012. Revealing substituent effects on the electronic structure and planarity of Ni-porphyrins. *Computational and Theoretical Chemistry* 981: 73-85.

Baseden, K.A. & Tye, J.W. 2014. Introduction to density functional theory: Calculations by hand on the helium atom. *Journal of Chemical Education* 91(12): 2116-2123.

Bashir, B., Alotaibi, M.M. & Clayborne, A.Z. 2024. Computational investigation of structural, electronic and spectroscopic properties of Ni and Zn metalloporphyrins with varying anchoring groups. *Journal of Chemical Physics* 160(13): 134305.

Becke, A.D. 1993. Density-functional thermochemistry. III. The role of exact exchange. *The Journal of Chemical Physics* 98(7): 5648-5662.

Bouicha, M.A., Mabrouk, C., Gassoumi, B., Barhoumi, H., Molton, F., Loiseau, F., Roisnel, T., Medina, A.S., Cornejo Bravo, J.M., Lopez-Maldonado, E.A. & Nasri, H. 2025. New zinc(ii) metalloporphyrin: Molecular structure, spectroscopic characterization, electrochemical sensing of dopamine and catalytic dye degradation. *RSC Advances* 15(13): 9810-9827.

Dhifaoui, S., Azaid, A., Bourass, M., Hassen, L.B.H., Nasri, H. & Bouachrine, M. 2021. DFT studies on molecular structure, absorption properties, NBO analysis, and Hirshfeld surface analysis of iron(III) porphyrin complex. *Physical Chemistry Research* 9(4): 701-713.

Fischer, H. 1930. *On Haemin and the Relationships Between Haemin and Chlorophyll*. Nobel Lecture, Nobel Prize in Chemistry 1930. Amsterdam: Elsevier Publishing Company.

Giovannetti, R. 2012. The use of spectrophotometry UV-Vis for the study of porphyrins. In *Macro to Nano Spectroscopy*, edited by Uddin, J. Intech.

Higashino, T., Kawamoto, K., Sugiura, K., Fujimori, Y., Tsuji, Y., Kurotobi, K., Ito, S. & Imahori, H. 2016. Effects of bulky substituents of push-pull porphyrins on photovoltaic properties of dye-sensitized solar cells. *ACS Applied Materials and Interfaces* 8(24): 15379-15390.

Kuan, C-H., Mai, C-L., Saravanan, V., Lin, T-C., Shih, Y-S., Kuo, C-H., Tsai, M-C., Yeh, C-Y. & Diau, E.W-G. 2025. Development of double fence porphyrins as self-assembled monolayers for tin-based perovskite solar cells. *Small* 21(27): 2504259.

Lee, C., Yang, W. & Parr, R.G. 1988. Development of the Colle-Salvetti correlation-energy formula into a functional of the electron density. *Physical Review B* 37(2): 785-789.

Lin, Y., Zhou, T., Bai, R. & Xie, Y. 2020. Chemical approaches for the enhancement of porphyrin skeleton-based photodynamic therapy. *Journal of Enzyme Inhibition and Medicinal Chemistry* 35(1): 1080-1099.

Lindsey, J.S. 2010. Synthetic routes to meso-patterned porphyrins. *Accounts of Chemical Research* 43(2): 300-311.

Lindsey, J.S., Schreiman, I.C., Hsu, H.C., Kearney, P.C. & Marguerettaz, A.M. 1987. Rothemund and Adler-Longo reactions revisited: Synthesis of tetraphenylporphyrins under equilibrium conditions. *Journal of Organic Chemistry* 52(5): 827-836.

Nishida, K., Tojo, T., Kondo, T. & Yuasa, M. 2021. Evaluation of the correlation between porphyrin accumulation in cancer cells and functional positions for application as a drug carrier. *Scientific Reports* 11(1): 2046.

Nuur Haziqah Mohd Radzuan, Zaitun Ghazali, Nurul Izzaty Hassan, Mohd Bakri Bakar, Siti Aishah Hasbullah & Muntaz Abu Bakar. 2025. Synthesis and characterization of 5,15 A2-type porphyrin, metalloporphyrin and preliminary study on carbon dioxide adsorption. *Sains Malaysiana* 54(6): 1535-1549.

Nuur Haziqah Mohd Radzuan, Nur Aqilah Zahirah Norazmi, Amatul Hamizah Ali, Muntaz Abu Bakar, Hani Kartini Agustar, Mohd Ridzuan Mohd Abd Razak & Nurul Izzaty Hassan. 2021. Synthesis, *in vitro* antiplasmodial activity and cytotoxicity of metalloporphyrins against *Plasmodium falciparum* K1. *Sains Malaysiana* 50(10): 2945-2956.

Parr, R.G. & Pearson, R.G. 1983. Absolute hardness: Companion parameter to absolute electronegativity. *Journal of the American Chemical Society* 105(26): 7512-7516.

Qu, C., Gong, X., Sun, Y., Gao, H., Cai, F., Zhao, Y., Wu, F. & Shen, Z. 2024. Synergistic meso-β regulation of porphyrins: Squeezing the band gap into the near-infrared I/II region. *Chemical Science* 15(27): 10491-10498.

Sánchez-Bojorge, N.A., Zaragoza-Galán, G., Flores-Holguín, N.R., Chávez-Rojo, M.A., Castro-García, C. & Rodríguez-Valdez, L.M. 2019. Theoretical analysis of the electronic properties in zinc-porphyrins derivatives. *Journal of Molecular Structure* 1191: 259-270.

Senge, M.O. 2011. Stirring the porphyrin alphabet soup—Functionalization reactions for porphyrins. *Chemical Communications* 47(7): 1943-1960.

Tahoun, M., Gee, C.T., McCoy, V.E., Sander, P.M. & Müller, C.E. 2021. Chemistry of porphyrins in fossil plants and animals. *RSC Advances* 11(13): 7552-7563.

Vicente, M. & Smith, K. 2014. Syntheses and functionalizations of porphyrin macrocycles. *Current Organic Synthesis* 11(1): 3-28.

Walker, M., Harvey, A.J.A., Sen, A. & Dessent, C.E.H. 2013. Performance of M06, M06-2X, and M06-HF density functionals for conformationally flexible anionic clusters: M06 functionals perform better than B3LYP for a model system with dispersion and ionic hydrogen-bonding interactions. *Journal of Physical Chemistry* 117(47): 12590-12600.

Wan Nurfadhilah Zaharim, Shukri Sulaiman, Risdiana, Lusi Safriani & Rizafizah Othaman. 2024. Kajian teori fungsian ketumpatan pada struktur, tapak perangkap muon dan interaksi hiperhalus muon dalam poli(3-heksiltiofena-2,5-dil). *Sains Malaysiana* 53(10): 3315-3326.

Williams, D.B.G. & Lawton, M. 2010. Drying of organic solvents: Quantitative evaluation of the efficiency of several desiccants. *Journal of Organic Chemistry* 75(24): 8351-8354.

Zhang, Y., Higashino, T., Namikawa, K., Osterloh, W.R. & Imahori, H. 2025. Chemical science molecular engineering of porphyrin dyes and copper complexes for enhanced dye regeneration. *Royal Society of Chemistry* 16(33): 15004-15014.